Interaction of itinerant electrons and spin fluctuations in electron-doped cuprates

Seung Ryong Park,[1,2] Takao Morinari,[3] Dong Joon Song,[1] Choon Shik Leem,[1] Chul Kim,[1] Sung Kyun Choi,[1,*] Kyujin Choi,[1] Jae Hoon Kim,[1] Felix Schmitt,[4,5] Sung Kwan Mo,[6] Dong Hui Lu,[7] Zhi-Xun Shen,[4,5] Hiroshi Eisaki,[8] Takami Tohyama,[3,9] Jung Hoon Han,[10,11] and Changyoung Kim[1,†]

[1]*Institute of Physics and Applied Physics, Yonsei University, Seoul 120-749, Korea*

[2]*Department of Physics, University of Colorado at Boulder, Boulder, Colorado 80309, USA*

[3]*Yukawa Institute for Theoretical Physics, Kyoto University, Kyoto 606-8502, Japan*

[4]*Stanford Institute of Materials and Energy Sciences, Stanford University, Stanford, California 94305, USA*

[5]*Departments of Physics and Applied Physics, and Geballe Laboratory for Advanced Materials, Stanford University, Stanford, California 94305, USA*

[6]*Advanced Light Source, Lawrence Berkeley National Lab, Berkeley, California 94720, USA*

[7]*Stanford Synchrotron Radiation Lightsource, SLAC National Accelerator Laboratory, Menlo Park, California 94025, USA*

[8]*Nanoelectronics Research Institute, AIST, Tsukuba, Ibaraki 305-8568, Japan*

[9]*JST Transformative Research-Project on Iron Pnictides (TRIP), Chiyoda, Tokyo 102-0075, Japan*

[10]*Department of Physics and BK21 Physics Research Division, Sungkyunkwan University, Suwon 440-746, Korea*

[11]*Asia Pacific Center for Theoretical Physics, POSTECH, Pohang, Gyeongbuk 790-784, Korea*

(Received 2 January 2013; revised manuscript received 14 May 2013; published 31 May 2013)

We performed angle-resolved photoemission and optical studies on electron-doped high-temperature superconductors (HTSCs), and compared the results with various theoretical models. Based on the fit to the experimental data, we conclude that itinerant electrons in the nonmagnetic phase predominantly couple to the phase fluctuations of the remnant antiferromagnetic (AF) order, rather than to the spin excitations derived from particle-hole pairs. Our observation naturally accounts for the pseudogap phenomenon and other experimental facts in electron-doped HTSCs in terms of the size of the remnant moment and the AF-correlation length. We propose a microscopic model based on the phase fluctuation scenario which leads to a d-wave pairing gap.

DOI: 10.1103/PhysRevB.87.174527 PACS number(s): 74.72.Ek, 74.20.−z, 74.25.Gz, 74.25.Jb

I. INTRODUCTION

The parent compounds of novel superconductors such as high-temperature superconductors (HTSCs) and heavy-fermion (HF) and recently discovered Fe-based superconductors possess antiferromagnetism (AF) and only become superconductors either under the application of pressure or when carriers are doped through substitution of elements, which concomitantly weakens AF ordering.[1–3] When AF order is absent, spin fluctuations still remain, even well into the superconducting phase,[4–7] and are believed to play a key role in bringing on superconductivity.[2,8,9] In light of such general observation, it is of utmost importance to have a precise characterization of the so-called spin fluctuations and establish a quantitative connection to superconductivity. A recent such success is the work of Dahm *et al.*[9] which quantitatively related the measured spin susceptibility spectrum to the transition temperature of hole-doped HTSCs.

Spectroscopic methods such as angle-resolved photoemission (ARPES)[9,10] and optical spectroscopy[11] experiments have been extensively performed to unravel the mechanism of electron-spin fluctuation interactions in HTSCs and Fe-based superconductors, because the observed spectral functions, which reveal electron dynamics in the frequency domain, should include signatures of interactions between electrons and other excitations such as spin fluctuations,[10,11] and provide a way to find the microscopic model of the interaction through comparison studies with model simulations. However, interpretation of observed spectral features can be severely hampered when there are multiple bands (as in Fe-based superconductors) or if several excitations with comparable energy scales coexist. In hole-doped HTSCs, superconducting gaps and pseudogaps, phonons, and spin resonance modes all have similar energies of several tens of meV.[10]

On the other hand, electron-doped HTSCs are free from these problems as they come with a single band and well-separated energy scales. Known energies of superconducting gap,[12–15] spin resonance mode,[5] ARPES kink[16] and pseudogap,[17–21] are about 3, 10, 60, and 200 meV, respectively. The kink structures in ARPES spectra at 60 meV were shown to be due to phonons,[16] while pseudogaps are believed to be due to magnetism.[6,22] The pseudogap energy is well separated from other energy scales and the superconducting gap is rather small. Electron-doped HTSCs, therefore, provide a unique opportunity to examine the nature of the electron-spin fluctuations by spectroscopic methods. Furthermore, strong evidence for superconductivity mediated by spin fluctuations in electron-doped HTSCs has been found recently through doping-dependent transport studies across the superconducting dome boundary.[23]

Theoretical studies have been performed in order to understand the electron-spin fluctuation interactions and the pesudogap in electron-doped HTSCs. Mean-field calculations for electron-doped $t-t'-t''-U$ and $t-t'-t''-J$ models show AF ground state.[25,26] Local density approximation (LDA) + dynamical mean-field theory (DMFT) calculations also give AF ground state even with electron doping up to about 20%,[27] and the calculated ARPES spectral functions from LDA + DMFT show clear back-folding of bands at the antiferromagnetic zone boundary (AFZB).[27] Even though short-range AF fluctuations are additionally introduced into

LDA + DMFT calculation,[28,29] the back-folding of bands still remains, whereas ARPES data do not show it.[14,19] Many-body calculations for the $t - t' - t'' - U$ model beyond the mean-field approaches give good agreement with experimentally observed spin correlation length and pseudogap in $Nd_{2-x}Ce_xCuO_4$.[22] It is, however, crucial to develop an effective Hamiltonian directly describing electron-spin fluctuation interactions, since the effective Hamiltonian can give deep insight about the electron-spin fluctuation interactions as well as superconductivity in the electron-doped HTSCs.

In this article, we report the temperature, doping, and material dependence of the pseudogap in the electron-doped cuprates by ARPES and optical spectroscopy. Remarkably, all spectroscopic data show the same size of pseudogap, regardless of temperature and doping concentration, but the spectral weight fills up within the gap region, as the AF-correlation length decreases. The pseudogap feature in the electron-doped HTSCs is clearly beyond the $\sqrt{2} \times \sqrt{2}$ band reconstruction model based on long-range AF order. We propose an effective model including the AF-phase fluctuations. This model has only a single free parameter to fit with ARPES and optical conductivity data and reproduces our spectroscopic data very well.

II. EXPERIMENTAL DETAILS

Single crystals of $Nd_{2-x}Ce_xCuO_4$ (NCCO, $x = 0.15$), $Sm_{2-x}Ce_xCuO_4$ (SCCO, $x = 0.10$, 0.15, 0.18) and $Eu_{2-x}Ce_xCuO_4$ (ECCO, $x = 0.15$) were grown by the traveling-solvent floating-zone method. The crystals were annealed in Ar for 48 hours at about 900 °C to induce superconductivity. Superconducting transition temperatures, which are measured by magnetic susceptibility measurements, are 24, 13, 10, and below 2 K for NCCO, SCCO ($x = 0.15$), SCCO ($x = 018$), and ECCO, respectively.

The ARPES data of NCCO and SCCO were obtained at the beamline 5-4 of Stanford Synchrotron Radiation Laboratory and beamlines 7.0.1 and 10.0.1 of the Advanced Light Source. Photon energies of 16.5, 55, and 85 eV were used. Samples were cleaved *in situ*. The base pressure was better than 5×10^{-11} torr. The experimental temperature for SCCO and ECCO was kept at 10 K while that for NCCO was varied between 10 and 280 K. The total energy resolution used for the presented data was typically 14 meV and the angular resolution was 0.25°.

The infrared conductivity data from NCCO, SCCO, and ECCO were obtained through normal-incidence in-plane reflectivity measurements with Bruker 113v and Bruker 120HR Fourier-transform infrared spectrometers. The single-crystal samples were coated with Au *in situ* for reference measurements and the resulting data were converted into conductivity via a Kramers-Kronig analysis. The temperature was varied from 10 to 300 K by placing the samples within an optical cryostat.

III. RESULTS AND DISCUSSION

A. Experimental results

Figure 1(a) shows a plot of AF-correlation length, reproduced from previous neutron scattering work on NCCO.[6] Moving away from AF order (by increase either temperature or doping) causes a rapid decrease in the correlation length. On the other hand, μSR experiments showed that replacing Nd by Sm and Eu in NCCO progressively enhances the spin ordering.[24] Therefore, one may investigate the effect of AF-correlation length on the electronic spectral functions through systematic variation of temperature, rare-earth element substitution, and doping.

We first look at optical conductivities of electron-doped materials, where the pseudogap feature is manifested as a dip in the frequency-dependent conductivity.[21] Figure 1(b) plots rare-earth element and temperature dependent optical conductivities. The temperature-dependent data show that the pseudogap feature gradually disappears as the temperature increases. Optical conductivity of optimally doped NCCO shows a very weak, if any, pseudogap feature as reported earlier.[21] Then, substitution of Nd by Sm makes the pseudogap feature in the optical conductivity stronger (and by Eu even stronger). In combination with previous reports on the doping-dependent pseudogap effect,[21] these experimental findings point to the pseudogap effect growing stronger with enhanced AF correlations. However, there is little difference in the pseudogap size [the peak position indicated by the arrows in Fig. 1(b)], in spite of a large variation in the overall pseudogap effect.

In ARPES, pseudogap features are observed as the suppression of spectral weights at the Fermi energy at the momentum space locations where the original Fermi surface (FS) crosses the AFZB[17] (also known as hot spots). Figures 1(c)–1(e) show FS maps of SCCO ($x = 0.15$) and NCCO ($x = 0.15$). For the 10 K data, a clear suppression of spectral weight is observed in both SCCO and NCCO. Comparison of the SCCO and NCCO data taken at 10 K show that the pseudogap effect is smaller for NCCO. Increase of temperature results in even smaller pseudogap effect, seen as a more connected FS in the NCCO's 280 K data. The trend in the pseudogap effect with varying temperature and rare-earth element substitution is consistent with that in the optical data in Fig. 1(b).

One may further investigate the pseudogap effect by looking at the AFZB cut as marked by the solid arrow in Fig. 1(c). AFZB data from SCCO and NCCO are plotted in Figs. 1(f)–1(h). There are two parallel bands along this direction as reported earlier.[19] These split bands can be roughly accounted for by an extra $\sqrt{2} \times \sqrt{2}$ order.[18,19] In addition, the pseudogap effect (spectral weight suppression at the arrows) becomes less prominent as the doping increases or as Sm is replaced by Nd.

Energy distribution curves (EDCs) reveal more detailed information on the pseudogap effect. Rare-earth, doping, and temperature-dependent EDCs from a hot spot [shown by the circle in Fig. 1(d)] are plotted in Figs. 1(i)–1(k). The NCCO data in Fig. 1(i) show a stronger Fermi edge than the SCCO data while the peak position in the EDC more or less stays near 0.15 eV. The same trend is there for the doping dependence depicted in Fig. 1(j). The Fermi edge grows with the doping while the peak position does not change as much. Doping-dependent data from NCCO also show similar results.[20] The most convincing evidence for such behavior comes from the temperature dependence. Unlike doping and rare-earth substitution, which affect various parameters in addition to the AF-correlation length,[30] temperature-dependent

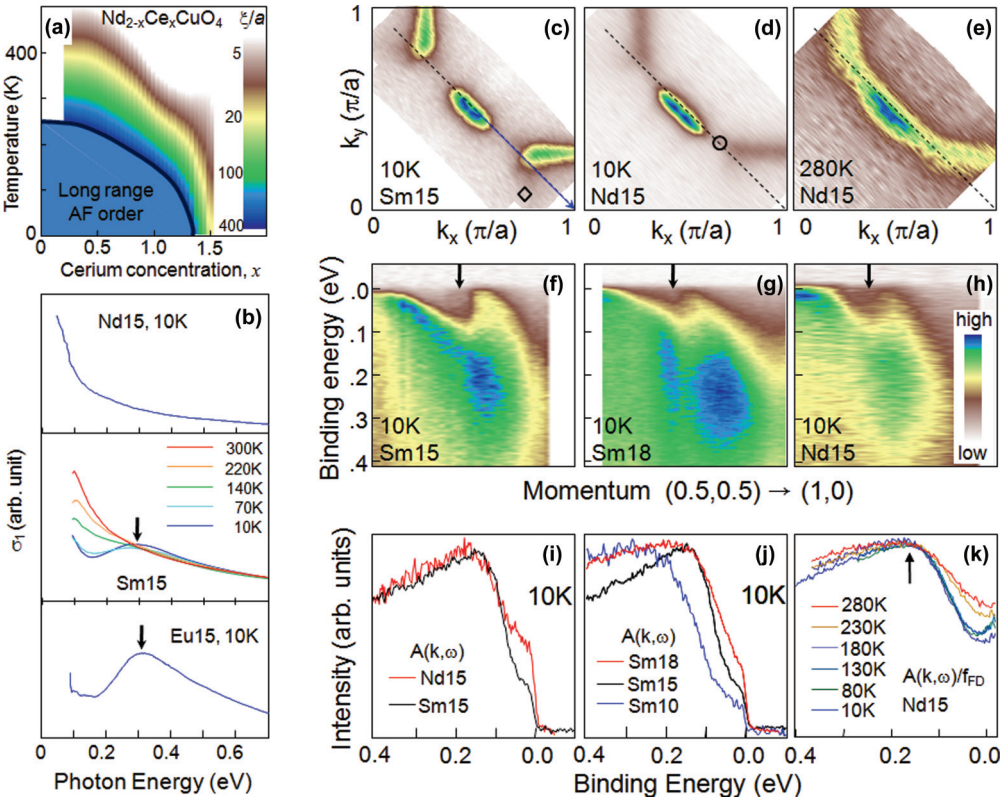

FIG. 1. (Color online) (a) AF-correlation length as functions of doping and temperature reproduced from Motoyama *et al.* (Ref. 6). (b) Rare-earth and temperature-dependent optical conductivity from electron-doped HTSCs. Optical conductivity for SCCO (middle) is reproduced from Park *et al.* (Ref. 19). The arrows indicate the pseudogap energy scale. For clarity, only the conductivity above the phonon energy is presented. (c) FS map of SCCO. (d) and (e) FS maps of NCCO at 10 K and 280 K, respectively. The dotted lines depict the AFZB. The empty circle indicates hot spot in (d). (f) ARPES spectra along the AFZB cut for SCCO ($x = 0.15$), (g) for SCCO ($x = 0.18$), and (h) for NCCO ($x = 0.15$). Hot spot EDCs are plotted for (i) different rare-earth elements and (j) dopings. (k) Temperature-dependent hot spot EDCs. $A(k,\omega)$ divided by the Fermi function is plotted instead of $A(k,\omega)$ for clarity.

studies offer a more direct approach to the investigation of the AF correlations. Temperature-dependent EDCs from hot spots are divided by the Fermi Dirac distribution function to remove the thermal broadening effect and plotted in Fig. 1(k). The most striking aspect of the data is that the pseudogap size (arrow in the figure) remains insensitive to temperature. Instead, the pseudogap is gradually filled up with increasing temperature. The temperature dependence of the pseudogap evolution is independent of measurement procedures.

To summarize, our ARPES and optical conductivity experiments show that weakened AF correlations in electron-doped HTSCs result in filling up of the pseudogap instead of closing, and leaves the pseudogap energy scale nearly intact.

B. Comparison with a long-range AF order model

As mentioned above, the overall experimental band dispersion is roughly compatible with the band structure due to an extra $\sqrt{2} \times \sqrt{2}$ order arising from long-range AF order.[25,26] One expects that the AF order will cause both band folding about the AFZB and formation of a folded Fermi surface. However, as one can see in Fig. 1(c) (for example, see where an open diamond is), the intensity of folded FS is much weaker than what is expected within such a model. More seriously, our data show that bands do not fold back at the AFZB but extend beyond it. Figures 2(a) and 2(b) show experimental data from NCCO ($x = 0.15$) and SCCO ($x = 0.15$) along the dashed arrow cut in Fig. 2(d). Even though two bands are observed as expected in the model, the lower band extends beyond the AFZB (dashed line). This is in sharp contrast to the simulation result in Fig. 2(c) in which bands are folded about the AFZB. Yet another discrepancy is the finite Fermi energy spectral weight at the hot spot [Figs. 1(i)–1(k)]. This is forbidden in a long-range AF model due opening of a full gap. These observations point out the inadequacy of a long-range AF order model in interpreting the pseudogap features.

C. Comparison with a spin-fermion model

The main problem with the long-range AF order scenario is its inability to account for the fluctuations. One may thus instead look at the spin-fermion model,[31–33] commonly used to explain non-Fermi-liquid behavior and the d-wave superconducting order parameter of electron-doped cuprates.[34,35] The spin-fermion model assumes electronic spin coupling to the bosonic-spin-fluctuation mode $\mathbf{S}_q$ in the form[31–33] $H_{sf} = g_{sf} \sum_{k,q} c^{\dagger}_{k+q,\alpha}(\boldsymbol{\sigma})_{\alpha\beta} c_{k,\beta} \cdot \mathbf{S}_q$. The strength of spin-fermion coupling g_{sf} is typically assumed constant independently of

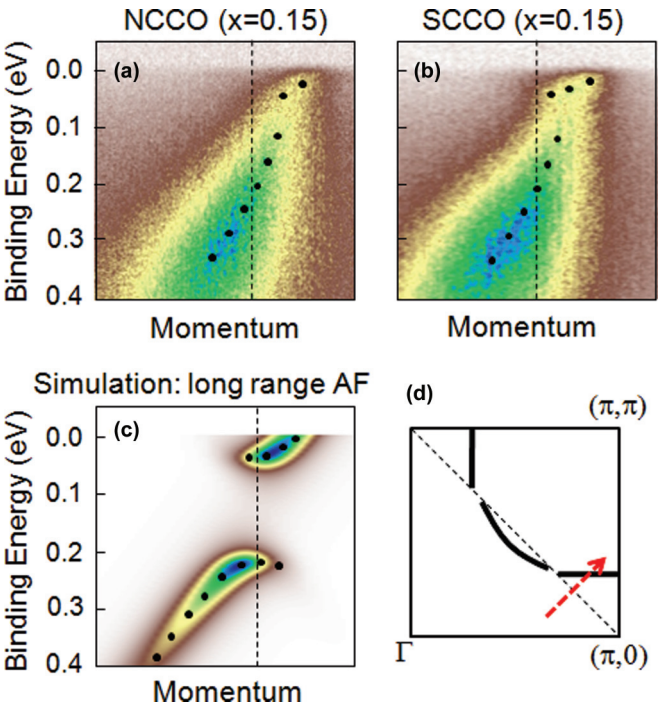

FIG. 2. (Color online) Experimentally observed spectral functions of (a) NCCO ($x = 0.15$) and (b) SCCO ($x = 0.15$) along dashed red arrow in (d). Spectral function for SCCO is reproduced from Park *et al.* (Ref. 19). (c) Spectral function from $\sqrt{2} \times \sqrt{2}$ reconstruction model along the dashed red arrow in (d). (d) Schematic FS of electron-doped cuprates in a quarter of the Brillouin zone. Dotted lines in (a)–(d) indicate the AFZB.

the scattering momenta involved. Electron creation (annihilation) operators are $c_k^\dagger$ (c_k) and $\boldsymbol{\sigma}$ is the Pauli matrix. In our work, we assume isotropy of the scattering channels among the x, y, and z directions and keep only one boson species $S_q^x \equiv a_q$ and analyze the Hamiltonian

$$H = \sum_{k\sigma} \varepsilon_k c_{k\sigma}^\dagger c_{k\sigma} + \sum_q \omega_q a_q^\dagger a_q + g_{sf} \sum_q [(c_{k+p,\downarrow}^\dagger c_{k,\uparrow} + c_{k+p,\uparrow}^\dagger c_{k,\downarrow}) a_q + \text{H.c.}]. \quad (1)$$

The band electronic dispersion and the spin spectrum are denoted ε_k and ω_q, respectively.

The electronic Matsubara Green's function $G(k,i\omega)$ for momentum k and imaginary frequency $i\omega$ after one-loop self-energy correction from the spin-fermion coupling reads

$$G(k,i\omega) = 1/\big(\varepsilon_k - i\omega - \Sigma(k,i\omega)\big),$$
$$\Sigma(k,i\omega) = g_{sf}^2 \sum_{p,i\nu} (G_{k+p}(i\omega + i\nu) D_p(i\nu) + G_{k-p}(i\omega - i\nu) D_p(i\nu)). \quad (2)$$

The propagator for the bosonic mode at momentum q and imaginary frequency $i\nu$ is $D_q(i\nu)$. For the noninteracting bosons with the propagator $D_q(i\nu) = \omega_p - i\nu$, the frequency sum can be carried out to obtain the self-energy

$$\Sigma(k,i\omega) = g_{sf}^2 \left(\sum_p \frac{B(\omega_p) + F(\varepsilon_{k+p})}{\varepsilon_{k+p} - \omega_p - i\omega} + \sum_p \frac{B(\omega_p) + F(-\varepsilon_{k+p})}{\varepsilon_{k+p} + \omega_p - i\omega} \right). \quad (3)$$

The Bose and Fermi factors are introduced: $B(x) = 1/(e^{\beta x} - 1)$, $F(x) = 1/(e^{\beta x} + 1)$. In the zero-temperature limit all the Bose factors vanish, and $F(x)$ reduces to the step function, $F(x) = \theta(-x)$:

$$G^{-1}(k,\omega) = \varepsilon_k - \omega - i\Gamma - g_{sf}^2 \sum_p \left(\frac{\theta(\varepsilon_{k+p})}{\varepsilon_{k+p} + \omega_p - \omega - i\Gamma} + \frac{\theta(-\varepsilon_{k+p})}{\varepsilon_{k+p} - \omega_p - \omega - i\Gamma} \right). \quad (4)$$

The retarded Green's function above is obtained above with the rotation $i\omega \to \omega + i\Gamma$. Here Γ reflects the self-energy effects from impurities. The spin-fluctuation-mediated effects are only found in the self-energy part proportional to g_{sf}^2. For comparison with the ARPES data, the frequency of interest is on the negative side, $\omega < 0$, and both ε_k and ε_{k+Q} are negative as well. With this in mind, the first term in the self-energy drops out:

$$G^{-1}(k,\omega) \approx \varepsilon_k - \omega - i\Gamma - g_{sf}^2 \sum_p \frac{\theta(-\varepsilon_{k+p})}{\varepsilon_{k+p} - \omega_p - \omega - i\Gamma}. \quad (5)$$

A neutron scattering experiment on $Pr_{0.88}LaCe_{0.12}CuO_{4-\delta}$ (Ref. 36) suggests the existence of a localized magnon excitation ω_p where p is narrowly confined to $Q = (\pi,\pi)$ and furthermore ω_p does not disperse very much with variations in the momentum $p - Q$. Based on that experimental result, we follow the approach of Harrison *et al.*,[37] and introduce a statistical distribution for the momentum p:

$$\rho(p) = \frac{K}{\xi^{-2} + (p - Q)^2},$$
$$\int \frac{dp_x dp_y}{(2\pi)^2} \rho(p) \equiv \int dp \rho(p) = 1. \quad (6)$$

The Green's function in Eq. (5) becomes

$$G^{-1}(k,\omega) \approx \varepsilon_k - \omega - i\Gamma - g_{sf}^2 \times \int dp \rho(p) \frac{\theta(-\varepsilon_{k+p})}{\varepsilon_{k+p} - \omega_p - \omega - i\Gamma}. \quad (7)$$

The spectral function is the imaginary part of the retarded Green's function, $A(k,\omega) = (1/\pi)\text{Im}[G(k,\omega)]$.

The dispersion ε_k in the Green's function is taken from the tight-binding fit of the ARPES data obtained from SCCO. We previously found that the nearest-, next-nearest- and next-next-nearest-neighbor hopping matrices are $t = 0.238$, $t' = 0.06$, and $t'' = 0.025$ eV, respectively.[19] The chemical potential used gives the average electron doping of 15%.[19] We have used a momentum (p) independent spin excitation energy $\omega_p \approx 5$ meV although the final results turned out to be insensitive to the choice of the resonance energy within a

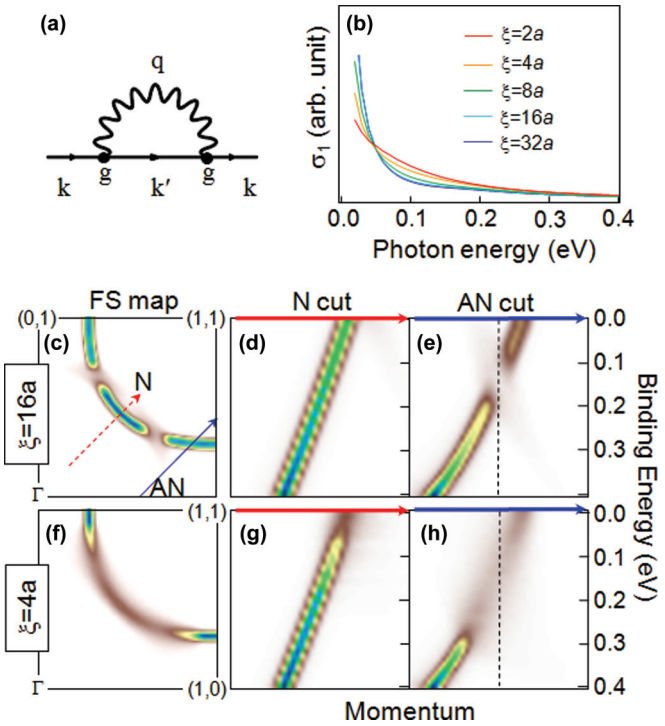

FIG. 3. (Color online) Simulated spectral functions within spin-fermion models. (a) Feynman diagram evaluated in the spin-fermion model with q the momentum of the spin excitation. (b) Calculated optical conductivity based on the spin-fermion model for various AF-correlation lengths. Calculated ARPES spectral functions based on the spin-fermion model are shown in panels (c)–(h). (c) FS map, (d) nodal cut [N, dotted line in panel (c)] and (e) antinodal cut [AN, solid line in panel (c)] for $\xi = 16a$. For $\xi = 4a$, (f) FS map, (g) N cut, and (h) AN cut are plotted.

few meV window. The impurity broadening Γ is typically chosen very small to minimize the extrinsic effect in the spectral function calculation. With only one fitting parameter g_{sf} left, we adjust the strength of spin-fermion coupling until a maximal fit of the ARPES spectral data to the calculated spectral function is achieved.

In this way, we find $g_{sf} \approx 0.1$ eV which is much smaller than the bandwidth of the electrons. It is then expected that a fully self-consistent approach[9] will yield similar results as the non-self-consistent calculation carried out here. Temperature, doping, and chemical substitution dependence of the antiferromagnetic correlation length is reflected in the momentum broadening factor, $\Delta p = \xi^{-1}$.

It is straightforward to calculate optical conductivity from $A(k,\omega)$. The real part of optical conductivity tensor $(\sigma^1_{\alpha\beta})$ in the linear response theory reads

$$\sigma^1_{\alpha\beta}(\omega) = \frac{\pi}{\omega}\sum_k v^\alpha_k v^\beta_k \int_{-\infty}^{\infty} dx \langle A_k(x)\rangle\langle A_k(x+\omega)\rangle \times [F(x) - F(x+\omega)]. \quad (8)$$

The velocity v^α_k is obtained as the momentum derivative of the bare dispersion ε_k in the absence of ordering, $v^\alpha_k = \partial\varepsilon_k/\partial k_\alpha$. $F(\varepsilon)$ is the Fermi function of energy ε. Averaging over x and y directions gives $\sigma^1(\omega) = \sigma^1_{xx}(\omega) + \sigma^1_{yy}(\omega)$.

The calculated optical conductivity plotted in Fig. 3(b) lacks the characteristic dip-hump feature (so conspicuous in the experimental data for large AF-correlation length).[31] In addition, there occurs spectral weight transfer from the Drude peak to the higher energy region between 0.05 and 0.2 eV in the simulated conductivity as the correlation length decreases (corresponding to temperature going up) even though such feature is absent in the experiments. Single-particle spectral functions depicted in Figs. 3(c)–3(h) show strong discrepancies as well. Calculated FSs in Figs. 3(c) and 3(f) for AF-correlation lengths $\xi = 16a$ and $\xi = 4a$ (where a is the lattice constant) look quite different from the experimental FSs plotted in Fig. 1. For example, the calculated FS for $\xi = 4a$ shows very weak spectral weight near $(\pi/2,\pi/2)$ in sharp contrast to the experimental one plotted in Fig. 1(e). In addition, the nodal cuts in Figs. 3(d) and 3(g) as well as the antinodal cuts in Figs. 3(e) and 3(h) do not show any folding effect about the AFZB. The overall effect from spin-fermion coupling appears as suppression of spectral weights, leaving little vestige of the $\sqrt{2} \times \sqrt{2}$ reconstruction. These observations lead us to conclude that coupling between electron and spin excitation in the sense of the spin-fermion model cannot account for the pseudogap effects seen in electron-doped HTSCs.

D. Comparison with an AF-phase fluctuation model

As discussed above, known models of electron-spin interaction fall short of capturing the observed quasiparticle spectral features in electron-doped HTSCs. A proper model accounting for the experimental features should realize two elements: (i) a robust pseudogap energy scale, which originates from local AF order and persists well into the magnetically disordered region, and (ii) fluctuations of localized moments. The interaction of itinerant electrons with such fluctuating local moments is expressed in the Hamiltonian

$$\boldsymbol{H} = \sum_{ij\sigma} t_{ij} c^+_{i\sigma} c_{j\sigma} + \lambda \sum_i m_i \cdot S_i, \quad (9)$$

where $c^+_{i\sigma}$ $(c_{i\sigma})$,t_{ij}, and λ are electron creation (annihilation) operator with spin $\sigma = \uparrow,\downarrow$, hopping energy, and a coupling constant, respectively. The spin S_i at site i is formed from the electron operators as $S^+_i = c^+_{i\uparrow}c_{i\downarrow}, S^-_i = c^+_{i\downarrow}c_{i\uparrow}$, and $S^z_i = \frac{1}{2}(c^+_{i\uparrow}c_{i\downarrow} - c^+_{i\downarrow}c_{i\uparrow})$, and is coupled to the local magnetic moment m_i. Here, we assume that spins are localized. This is not an unreasonable assumption for electron-doped cuprates, since itinerant spin-based calculations fail to reproduce experimentally observed spin excitations in electron-doped cuprates,[38] and the character of spin excitations in electron-doped cuprates does not change from underdoped to overdoped electron-doped cuprates, which is in clear contrast with holed-doped cuprates.[7] When both the magnitude and the orientation of AF ordered m_i are frozen, one obtains the long-range AF model. We introduce phase fluctuations from AF order to treat short-range AF correlations.

It is convenient to consider the magnetic moment axis lying in the xy plane when discussing the influence of phase fluctuations on electronic structure. This is a reasonable assumption, as the magnetic moment axis of electron-doped HTSCs was found to be in the xy plane.[39] Then one can rewrite

the Hamiltonian (9) as

$$\boldsymbol{H} = \sum_{ij\sigma} t_{ij} c^{+}_{i\sigma} c_{j\sigma} + \lambda \sum_{i} (m^{+}_{i} c^{+}_{i\downarrow} c_{i\uparrow} + m^{-}_{i} c^{+}_{i\uparrow} c_{i\downarrow}), \tag{10}$$

where $m^{+}_{i} = (m^{x}_{i} + i m^{y}_{i})/2$. Now the AF fluctuating moment is conveniently parameterized as $m^{+}_{i} = (-1)^{i} m e^{i\phi_i}$ with a space-time dependent phase ϕ_i. The correlation length ξ determines the spatial decay of the phase correlator, $\langle e^{i[\phi_i - \phi_j]} \rangle \propto e^{-r_{ij}/\xi}$, where r_{ij} measures the distance between sites. We assume that the time part of the phase ϕ_i is constant or so slowly varying that the local magnetic moments can be considered static within the time scale of photoemission process.[41]

To understand the effect of nonzero ϕ_i in a transparent manner, we first treat the case of a uniform momentum p shift $\phi_i = 2p \cdot r_i$.[40] Then, m^{+}_{i} is expressed as $(-1)^{i} m e^{2ip\cdot r_i}$, and Eq. (10) can be solved exactly after first carrying out the spin-dependent gauge transformation $c_{i\sigma} \rightarrow e^{-i\sigma p\cdot r_i} c_{i\sigma}$ in Eq. (10). The mean-field Hamiltonian, Eq. (10), in the new fermion basis becomes

$$H = {\sum_{k}}' \begin{pmatrix} c^{\dagger}_{k\uparrow} & c^{\dagger}_{k+Q\downarrow} \end{pmatrix} \begin{pmatrix} \varepsilon_{k+p} & \Delta \\ \Delta & \varepsilon_{k+Q-p} \end{pmatrix} \begin{pmatrix} c_{k\uparrow} \\ c_{k+Q\downarrow} \end{pmatrix} + {\sum_{k}}' \begin{pmatrix} c^{\dagger}_{k\downarrow} & c^{\dagger}_{k+Q\uparrow} \end{pmatrix} \begin{pmatrix} \varepsilon_{k-p} & \Delta \\ \Delta & \varepsilon_{k+Q+p} \end{pmatrix} \begin{pmatrix} c_{k\downarrow} \\ c_{k+Q\uparrow} \end{pmatrix} \tag{11}$$

over the reduced Brillouin zone $\sum'$ in momentum space. The bare band structure in the absence of ordering and phase fluctuations is ε_k, and $\Delta = \lambda m$ gives the gap opening due to AFM order at $Q = (\pi,\pi)$. After diagonalization, we obtain the Hamiltonian

$$H = {\sum_{k\sigma}}' E^{+}_{k\sigma} u^{\dagger}_{k\sigma} u_{k\sigma} + {\sum_{k\sigma}}' E^{-}_{k\sigma} d^{\dagger}_{k\sigma} d_{k\sigma} \tag{12}$$

with the set of energies

$$\begin{aligned} E^{\pm}_{k\uparrow} &= \tfrac{1}{2}(\varepsilon_{k+p} + \varepsilon_{k+Q-p}) \pm \sqrt{\Delta^2 + \tfrac{1}{4}(\varepsilon_{k+p} - \varepsilon_{k+Q-p})^2}, \\ E^{\pm}_{k\downarrow} &= \tfrac{1}{2}(\varepsilon_{k-p} + \varepsilon_{k+Q+p}) \pm \sqrt{\Delta^2 + \tfrac{1}{4}(\varepsilon_{k-p} - \varepsilon_{k+Q+p})^2}. \end{aligned} \tag{13}$$

Keeping in mind that the electron operator is written in the composite form $c_{i\sigma} e^{i\sigma p\cdot r_i}$, one can derive the spectral function as the imaginary part of the retarded Green's function $A_k(\omega, p) = (1/\pi)\mathrm{Im}[G_k(\omega + i\delta, p)]$ for a given phase shift p as

$$\begin{aligned} A_k(\omega, p) = {} & \cos^2\theta_{k-p,\uparrow} \delta(E^{+}_{k-p,\uparrow} - \omega) + \sin^2\theta_{k-p,\uparrow} \delta(E^{-}_{k-p,\uparrow} - \omega) \\ & + \cos^2\theta_{k+p,\downarrow} \delta(E^{+}_{k+p,\downarrow} - \omega) \\ & + \sin^2\theta_{k+p,\downarrow} \delta(E^{-}_{k+p,\downarrow} - \omega), \end{aligned} \tag{14}$$

along with the form factors

$$\begin{aligned} \cos 2\theta_{k-p,\uparrow} &= \frac{\varepsilon_k - \varepsilon_{k+Q-2p}}{\sqrt{(\varepsilon_k - \varepsilon_{k+Q-2p})^2 + 4\Delta^2}}, \\ \cos 2\theta_{k+p,\downarrow} &= \frac{\varepsilon_k - \varepsilon_{k+Q+2p}}{\sqrt{(\varepsilon_k - \varepsilon_{k+Q+2p})^2 + 4\Delta^2}}. \end{aligned} \tag{15}$$

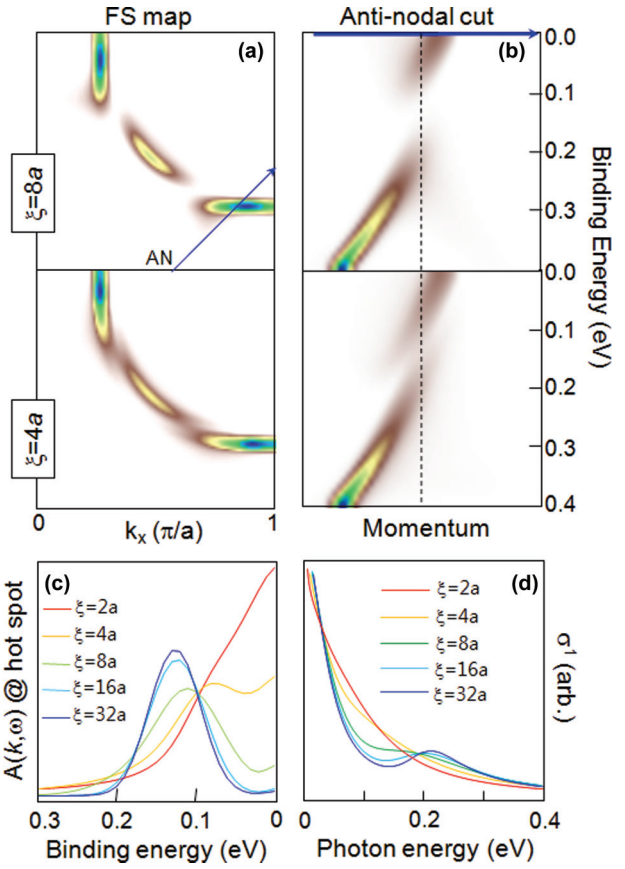

FIG. 4. (Color online) Calculated (a) FS maps and (b) spectral functions along blue arrow in (a) with various correlation lengths within AF-phase fluctuation model. (c) Hot spot EDCs for various AF phase correlation lengths. (d) Calculated optical conductivity within AF-phase fluctuation model for various AF phase correlation lengths.

The p-averaged spectral function $\langle A_k(\omega) \rangle$ is obtained as the weighted average of the above $A_k(\omega, p)$ with the distribution $\rho(p) = (\xi/\pi)(p^2\xi^2 + 1)^{-1}$:

$$\langle A_k(\omega) \rangle = \int \rho(p) A_k(\omega, p) d^2p = \frac{\xi}{\pi} \int \frac{A_x(\omega, p)}{p^2\xi^2 + 1} d^2p. \tag{16}$$

The correlation length ξ is thought to depend on temperature, doping, and chemical substitution. We note that ξ is a quantity measurable by neutron scattering experiments, as shown in Fig. 1(a). The only free parameter in this equation to fit our ARPES and optical conductivity is λm, which is equal to Δ (a half of pseudogap size).

Calculated single-particle spectral functions convoluted with experimental resolutions and optical conductivities for various AF-correlation lengths are plotted in Fig. 4. We used a tight-binding model with the nearest ($t = 0.238$ eV), the second nearest ($t' = 0.06$ eV), and the third nearest neighbor hopping ($t'' = 0.025$ eV) for the bare electron energy (ε_k).[19] We extracted λm of 0.1 eV through fitting to our data. Figure 4(a) shows the FS maps for $\xi = 8a$ and $4a$, where a is the lattice constant. One observes that the FS contour gets more connected as the correlation length becomes shorter. Moreover, spectral functions along the antinodal (AN) cut near the antinodal region in Fig. 4(b) show that, for short AF-correlation

lengths, the bands are not folded at the AFZB but extend into the next zone as was observed in the experimental data [Figs. 2(a), 2(b)].

To see the pseudogap behavior more clearly as a function of the AF-correlation length, we plot the EDCs at the hot spot for various AF-correlation lengths in Fig. 4(c). The peak around 0.12 eV is the position of the lower band at the hot spot. Unlike the experimental data, it appears peaky because simulation results do not have the typical background that exists in the experimental data. As the correlation length becomes shorter, the spectral weight at the Fermi energy grows and fills up the pseudogap, as was experimentally observed. The pseudogap size (twice the distance between the peak and the Fermi energy) does not change appreciably until the correlation length becomes very short and two bands eventually merge together, becoming one band at the Fermi energy.

We also test the validity of the model against experimental optical conductivity data. Calculated optical conductivities for various AF-correlation lengths are presented in Fig. 4(d). Optical conductivity for long correlation length (low temperature) shows the characteristic dip-hump feature around 0.15 and 0.23 eV, respectively. The spectral shape is strikingly similar to the low-temperature experimental data. As the AF-correlation length decreases, the dip-hump feature becomes weaker and eventually disappears.

An analogous behavior can be seen in the electronic states of lattice-ordered materials upon melting. The short-range correlations in atomic position persist above the melting temperature, and the band gap of the material becomes filled up (rather than closing).[42] This has been experimentally observed in thin films of lead just above the melting temperature.[42]

Is the microscopic origin of the AF-phase fluctuations an extrinsic or intrinsic property? It may be mainly an intrinsic property of electron-doped HTSCs in the sense of that the temperature-dependent AF-correlation length and pseudogap calculated from the $t-t'-t''-U$ model give good agreement with experimental observations[22] (although it is not straightforward to find origins of the itinerant electrons and the localized magnetic moments within the $t-t'-t''-U$ model). However, we believe that extrinsic properties such as defects should be taken into account as well, since pseudogap and the AF-correlation length strongly depend on rare-earth elements as well as temperature (Fig. 1). Defects in the Cu-O plane are inevitable during the oxygen-reducing process in electron-doped HTSCs.[43–45] Densities of the defects should be different for the different rare-earth elements. The defects may cause AF phase decoherence, which gives finite size of the AF-correlation length, and are the origin of rare-earth element dependence of AF-correlation length.

E. *d*-wave superconductivity from AF-phase fluctuations

As we have seen, many phenomenological features of electron-doped cuprates agree well with the model of phase-fluctuating local moments interacting with the spin of itinerant electrons. We now also ask whether the phase fluctuations can be the origin of superconductivity with $d_{x^2-y^2}$ symmetry order parameter. Here, we assume that the phase fluctuations, which are treated static in Sec. III D, also exist dynamically in spin excitations (essentially, spin excitations such as magnons, but with short correlation length). Indeed, broad peaks of inelastic magnetic neutron scattering in momentum space[36,46] support the phase fluctuation scenario at finite energy scale.

In order to derive the paring interaction mediated by the phase fluctuations, we will first parametrize the phase fluctuations as $m_i^+ = me^{i\phi_i}$. After carrying out the spin-dependent gauge transformation as in the previous section, we find the phase field dependent hopping Hamiltonian,

$$H_h = \sum_{i,j} t_{ij} e^{-i[\phi_i-\phi_j]/2} c^\dagger_{i,\uparrow} c_{j,\uparrow} + \sum_{i,j} t_{ij} e^{i[\phi_i-\phi_j]/2} c^\dagger_{i,\downarrow} c_{j,\downarrow}. \tag{17}$$

The remaining Hamiltonian responsible for local magnetic order, i.e., terms proportional to λ in Eq. (9), is dropped in the consideration of pairing interaction.

The effective interaction is obtained by expanding Eq. (17) with respect to the small angle difference $\phi_i - \phi_j$, and then integrating out the phase field. The energy dispersion of the phase field is taken as

$$\omega_q = \sqrt{c_{sw}^2[\sin^2(q_x - Q_x) + \sin^2(q_y - Q_y)] + \omega_0^2}. \tag{18}$$

The resulting effective interaction among electrons is

$$V = \sum_{k\neq k'} V_{k,k'} c^\dagger_{k',\uparrow} c^\dagger_{-k',\downarrow} c_{-k,\downarrow} c_{k,\uparrow}, \tag{19}$$

where

$$V_{k,k'} = \frac{\kappa(\varepsilon_k - \varepsilon_{k'})^2}{4\omega^2_{k+k'}}. \tag{20}$$

Here the parameter κ comes from the interaction between amplitude fluctuations of the localized moments. Through the canonical conjugate relationship between amplitude fluctuations and phase fluctuations, the phase field acquires dynamics parameterized by κ after integrating out amplitude fluctuations.

For simplicity we neglect retardation effects. The onset of superconductivity is analyzed within the standard BCS gap equation framework. We define the BCS gap function by

$$\Delta_k = \frac{1}{\Omega} \sum_{k'(\neq k)} V_{k,k'} \langle c_{-k',\downarrow} c_{k',\uparrow} \rangle, \tag{21}$$

with Ω the area of the system. The mean-field Hamiltonian is

$$H_{mf} = \sum_k \begin{pmatrix} c^\dagger_{k,\uparrow} & c_{-k,\downarrow} \end{pmatrix} \begin{pmatrix} \xi_k & \Delta_k \\ \Delta_k^* & -\xi_k \end{pmatrix} \begin{pmatrix} c_{k,\uparrow} \\ c^\dagger_{-k,\downarrow} \end{pmatrix}, \tag{22}$$

with $\xi_k = \varepsilon_k - \mu$. This Hamiltonian is diagonalized by the following Bogoliubov transformation:

$$\begin{pmatrix} c_{k,\uparrow} \\ c^\dagger_{-k,\downarrow} \end{pmatrix} = \begin{pmatrix} u_k & -v_k \\ v_k & u_k \end{pmatrix} \begin{pmatrix} \gamma_{k,\uparrow} \\ \gamma^\dagger_{-k,\downarrow} \end{pmatrix}, \tag{23}$$

where $u_k = (E_k + \xi_k)/\sqrt{2E_k(E_k+\xi_k)}$ and $v_k = \Delta_k/\sqrt{2E_k(E_k+\xi_k)}$ with $E_k = \sqrt{\xi_k^2 + |\Delta_k|^2}$. The onset of superconductivity is analyzed within the standard BCS gap equation framework. In the linearized form, the equation has

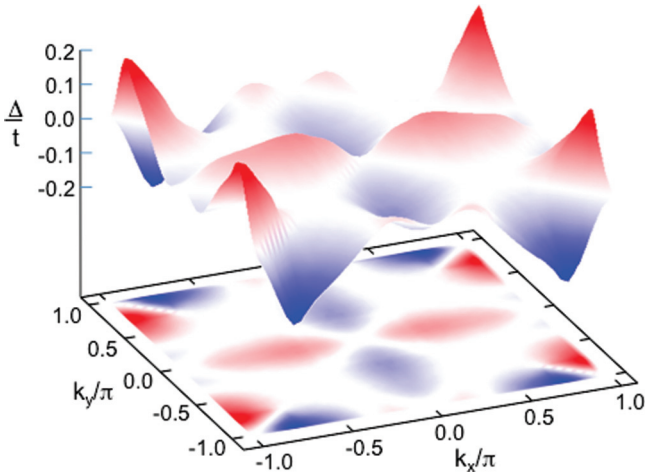

FIG. 5. (Color online) Superconducting gap function Δ_k from phase fluctuation model at 10% electron doping showing $d_{x^2-y^2}$ symmetry.

the form of an eigenvalue problem,

$$\Delta_k = -\eta \sum_{k' \neq k} \frac{V_{k,k'}}{2|\varepsilon_{k'} - \mu|} \tanh\left(\frac{\beta|\varepsilon_{k'} - \mu|}{2k_B T}\right)\Delta_{k'}, \quad (24)$$

where the gap function Δ_k is the eigenvector and η is the eigenvalue which becomes unity at the transition temperature. We assumed $c_{sw}/a = 0.5t, \kappa = 0.3t$, and $\omega_0 = 0.3t$ in solving the eigenvalue problem and used a 50×50 k-point mesh for the sum. With these parameters and at 10% electron doping, the transition temperature was found at $T_c/t = 0.03$. The gap function shown in Fig. 5 clearly shows that the gap symmetry is predominantly $d_{x^2-y^2}$.

The exercise carried out in this subsection is not meant to convince the reader that the origin of d-wave superconductivity is also the phase fluctuations, treated dynamically, of the magnetic order parameter. The point here is to merely emphasize that our proposed scenario of phase-disordered magnetic order parameter is consistent with the known d-wave pairing of superconductivity in electron-doped cuprates. It is reassuring, though, that d-wave pairing emerges naturally from our model as well as from other theories of pairing in electron-doped cuprates. Our observations of ARPES and optical conductivity can be fully understood within the context of static phase fluctuations of AF order.

IV. SUMMARY AND CONCLUSIONS

In summary, we showed that many aspects of temperature, doping, and rare-earth dependent ARPES spectral functions and optical conductivities in electron-doped HTSCs can be consistently accounted for by assuming interaction of electrons with the static phase fluctuations of AF order. A similar pseudogap phenomenon due to fluctuations of the phase degree of freedom occurs in other systems such as the liquid phase in the lead monolayer.[42] In our interpretation, the local moment size, proportional to the pseudogap energy, remains nearly constant although the degree of phase fluctuations as embodied in the correlation length depends sensitively on temperature, doping, and chemical substitution. Pairing of $d_{x^2-y^2}$ symmetry is derived within the phase fluctuation scheme in spin excitations. We propose this phase fluctuation scenario as a self-consistent scheme for the phenomenology of electron-doped HTSCs.

ACKNOWLEDGMENTS

S.R.P. thanks D. Parshall for helpful discussions. This work was supported by the KICOS (Grant No. K20602000008), Global Research Laboratory (Grant No. 2011-00329) through the National Research Foundation of Korea and the Converging Research Center Program (Grant No. 2012K001245) through the Ministry of Education, Science, and Technology. SSRL and ALS are operated by the DOE's Office of BES, Division of Materials Science. S.R.P. acknowledges support through the Seoul City government.

*Present address: Clarendon Laboratory, University of Oxford, Parks Road, Oxford OX1 3PU, United Kingdom.
†changyoung@yonsei.ac.kr

[1] M. A. Kastner, R. J. Birgeneau, G. Shirane, and Y. Endoh, Rev. Mod. Phys. **70**, 897 (1998).
[2] P. Gegenwart, Q. Si, and F. Steglich, Nat. Phy. **4**, 186 (2008).
[3] C. de la Cruz, Q. Huang, J. W. Lynn, J. Li, W. Ratcliff, J. L. Zarestky, H. A. Mook, G. F. Chen, J. L. Luo, N. L. Wang, and P. Dai, Nature (London) **453**, 899 (2008).
[4] S. M. Hayden, H. A. Mook, P. Dai, T. G. Perring, and F. Dogan, Nature (London) **429**, 531 (2004).
[5] S. D. Wilson, P. Dai, S. Li, S. Chi, H. J. Kang, and J. W. Lynn, Nature (London) **442**, 59 (2006).
[6] E. M. Motoyama, G. Yu, I. M. Vishik, O. P. Vajk, P. K. Mang, and M. Greven, Nature (London) **445**, 186 (2007).
[7] M. Fujita, M. Matsuda, S.-H. Lee, M. Nakagawa, and K. Yamada, Phys. Rev. Lett. **101**, 107003 (2008).
[8] P. Monthoux, D. Pines, and G. G. Lonzarich, Nature (London) **450**, 1177 (2007).
[9] T. Dahm, V. Hinkov, S. V. Borisenko, A. A. Kordyuk, V. B. Zabolotnyy, J. Fink, B. Büchner, D. J. Scalapino, W. Hanke, and B. Keimer, Nat. Phys. **5**, 217 (2009).
[10] A. Damascelli, Z. Hussain, and Z.-X. Shen, Rev. Mod. Phys. **75**, 473 (2003).
[11] D. N. Basov and T. Timusk, Rev. Mod. Phys. **77**, 721 (2005).
[12] N. P. Armitage, D. H. Lu, D. L. Feng, C. Kim, A. Damascelli, K. M. Shen, F. Ronning, Z.-X. Shen, Y. Onose, Y. Taguchi, and Y. Tokura, Phys. Rev. Lett. **86**, 1126 (2001).
[13] G. Blumberg, A. Koitzsch, A. Gozar, B. S. Dennis, C. A. Kendziora, P. Fournier, and R. L. Greene, Phys. Rev. Lett. **88**, 107002 (2002).
[14] H. Matsui, K. Terashima, T. Sato, T. Takahashi, M. Fujita, and K. Yamada, Phys. Rev. Lett. **95**, 017003 (2005).

[15]A. F. Santander-Syro, M. Ikeda, T. Yoshida, A. Fujimori, K. Ishizaka, M. Okawa, S. Shin, R. L. Greene, and N. Bontemps, Phys. Rev. Lett. **106**, 197002 (2011).

[16]S. R. Park, D. J. Song, C. S. Leem, Chul Kim, C. Kim, B. J. Kim, and H. Eisaki, Phys. Rev. Lett. **101**, 117006 (2008); F. Schmitt, W. S. Lee, D.-H. Lu, W. Meevasana, E. Motoyama, M. Greven, and Z.-X. Shen, Phys. Rev. B **78**, 100505 (2008).

[17]N. P. Armitage, D. H. Lu, C. Kim, A. Damascelli, K. M. Shen, F. Ronning, D. L. Feng, P. Bogdanov, Z.-X. Shen, Y. Onose, Y. Taguchi, Y. Tokura, P. K. Mang, N. Kaneko, and M. Greven, Phys. Rev. Lett. **87**, 147003 (2001).

[18]H. Matsui, K. Terashima, T. Sato, T. Takahashi, S.-C. Wang, H.-B. Yang, H. Ding, T. Uefuji, and K. Yamada, Phys. Rev. Lett. **94**, 047005 (2005).

[19]S. R. Park, Y. S. Roh, Y. K. Yoon, C. S. Leem, J. H. Kim, B. J. Kim, H. Koh, H. Eisaki, N. P. Armitage, and C. Kim, Phys. Rev. B **75**, 060501(R) (2007).

[20]H. Matsui, T. Takahashi, T. Sato, K. Terashima, H. Ding, T. Uefuji, and K. Yamada, Phys. Rev. B **75**, 224514 (2007).

[21]Y. Onose, Y. Taguchi, K. Ishizaka, and Y. Tokura, Phys. Rev. Lett. **87**, 217001 (2001); N. L. Wang, G. Li, D. Wu, X. H. Chen, C. H. Wang, and H. Ding, Phys. Rev. B **73**, 184502 (2006); A. Zimmers, J. M. Tomczak, R. P. S. M. Lobo, N. Bontemps, C. P. Hill, M. C. Barr, Y. Dagan, R. L. Greene, A. J. Millis, and C. C. Homes, Europhys. Lett. **70**, 225 (2005).

[22]B. Kyung, V. Hankevych, A.-M. Daré, and A.-M. S. Tremblay, Phys. Rev. Lett. **93**, 147004 (2004).

[23]K. Jin, N. P. Butch, K. Kirshenbaum, J. Paglione, and R. L. Greene, Nature (London) **476**, 73 (2011).

[24]T. Sasakawa (private communication).

[25]C. Kusko, R. S. Markiewicz, M. Lindroos, and A. Bansil, Phys. Rev. B **66**, 140513(R) (2002).

[26]Q. Yuan, Y. Chen, T. K. Lee, and C. S. Ting, Phys. Rev. B **69**, 214523 (2004).

[27]C. Weber, K. Haule, and G. Kotliar, Nat. Phys. **6**, 574 (2010).

[28]E. E. Kokorina, E. Z. Kuchinskii, I. A. Nekrasov, Z. V. Pchelkina, M. V. Sadovskii, A. Sekiyama, S. Suga, and M. Tsunekawa, JETP **107**, 828 (2008).

[29]I. A. Nekrasov, N. S. Pavlov, E. Z. Kuchinskii, M. V. Sadovskii, Z. V. Pchelkina, V. B. Zabolotnyy, J. Geck, B. Büchner, S. V. Borisenko, D. S. Inosov, A. A. Kordyuk, M. Lambacher, and A. Erb, Phys. Rev. B **80**, 140510(R) (2009).

[30]M. Ikeda, T. Yoshida, A. Fujimori, M. Kubota, K. Ono, Hena Das, T. Saha-Dasgupta, K. Unozawa, Y. Kaga, T. Sasagawa, and H. Takagi, Phys. Rev. B **80**, 014510 (2009).

[31]A. Abanov, A. V. Chubukov, and J. Schmalian, Adv. Phys. **52**, 119 (2003).

[32]P. Monthoux, A. V. Balatsky, and D. Pine, Phys. Rev. Lett. **67**, 3448 (1991).

[33]P. Monthoux and D. Pines, Phys. Rev. Lett. **69**, 961 (1992).

[34]D. Manske, I. Eremin, and K. H. Bennemann, Phys. Rev. B **62**, 13922 (2000).

[35]P. Krotkov and A. V. Chubukov, Phys. Rev. Lett. **96**, 107002 (2006).

[36]S. D. Wilson, S. Li, H. Woo, P. Dai, H. A. Mook, C. D. Frost, S. Komiya, and Y. Ando, Phys. Rev. Lett. **96**, 157001 (2006).

[37]N. Harrison, R. D. McDonald, and J. Singleton, Phys. Rev. Lett. **99**, 206406 (2007).

[38]F. Krüger, S. D. Wilson, L. Shan, S. Li, Y. Huang, H.-H. Wen, S.-C. Zhang, P. Dai, and J. Zaanen, Phys. Rev. B **76**, 094506 (2007).

[39]I. W. Sumarlin, J. W. Lynn, T. Chattopadhyay, S. N. Barilo, D. I. Zhigunov, and J. L. Peng, Phys. Rev. B **51**, 5824 (1995).

[40]M. Franz and A. J. Millis, Phys. Rev. B **58**, 14572 (1998).

[41]The time scale of photoemission process is determined by the relaxation time of the photohole and ranges from 10^{-15} to 10^{-12} seconds for strongly correlated materials.

[42]F. Baumberger, W. Auwärter, T. Greber, and J. Osterwalder, Science **306**, 2221 (2004).

[43]P. K. Mang, S. Larochelle, A. Mehta, O. P. Vajk, A. S. Erickson, L. Lu, W. J. L. Buyers, A. F. Marshall, K. Prokes, and M. Greven, Phys. Rev. B **70**, 094507 (2004).

[44]H. J. Kang, P. Dai, B. J. Campbell, P. J. Chupas, S. Rosenkranz, P. L. Lee, Q. Huang, S. Li, S. Komiya, and Y. Ando, Nat. Mater. **6**, 224 (2007).

[45]D. Song, S. R. Park, Chul Kim, Y. Kim, C. Leem, S. K. Choi, W. Jung, Y. Koh, G. Han, Y. Yoshida, H. Eisaki, D. H. Lu, Z.-X. Shen, and C. Kim, Phys. Rev. B **86**, 144520 (2012).

[46]G. Yu, Y. Li, E. M. Motoyama, K. Hradil, R. A. Mole, and M. Greven, Phys. Rev. B **82**, 172505 (2010).